Estimation of Forest Biophysical Characteristics in Northern Michigan with SIR-C/X-SAR

M. Craig Dobson, Fawwaz T. Ulaby, *Fellow, IEEE*, Leland E. Pierce, *Member, IEEE*, T. L. Sharik, K. M. Bergen, J. Kellndorfer, J. R. Kendra, E. Li, Y. C. Lin, A. Nashashibi, Kamal Sarabandi, *Senior Member, IEEE*, and P. Siqueira

Abstract—**A three-step process is presented for estimation of forest biophysical properties from orbital polarimetric SAR data. Simple direct retrieval of total aboveground biomass is shown to be ill-posed unless the effects of forest structure are explicitly taken into account. The process first involves classification by 1) using SAR data to classify terrain on the basis of structural categories or 2) *a priori* classification of vegetation type on some other basis. Next, polarimetric SAR data at L- and C-bands are used to estimate basal area, height and dry crown biomass for forested areas. The estimation algorithms are empirically determined and are specific to each structural class. The last step uses a simple biophysical model to combine the estimates of basal area and height with ancillary information on trunk taper factor and wood density to estimate trunk biomass. Total biomass is estimated as the sum of crown and trunk biomass.**

The methodology is tested using SIR-C data obtained from the Raco Supersite in Northern Michigan on Apr. 15, 1994. This site is located at the ecotone between the boreal forest and northern temperate forests, and includes forest communities common to both. The results show that for the forest communities examined, biophysical attributes can be estimated with relatively small rms errors: 1) height (0–23 m) with rms error of 2.4 m, 2) basal area (0–72 m^2/ha) with rms error of 3.5 m^2/ha, 3) dry trunk biomass (0–19 kg/m^2) with rms error of 1.1 kg/m^2, 4) dry crown biomass (0–6 kg/m^2) with rms error of 0.5 kg/m^2, and 5) total aboveground biomass (0–25 kg/m^2) with rms error of 1.4 kg/m^2. The addition of X-SAR data to SIR-C was found to yield substantial further improvement in estimates of crown biomass in particular. However, due to a small sample size resulting from antenna misalignment between SIR-C and X-SAR, the statistical significance of this improvement cannot be reliably established until further data are analyzed. Finally, the results reported herein are for a small subset of the data acquired by SIR-C/X-SAR. Future efforts will examine the role of incidence angle and environmental conditions on the retrieval process.

I. Introduction

A NUMBER of earth science disciplines require information on the spatial and temporal distribution of land cover types [1]. At local to regional scales, information on actual land-cover is obtained by a variety of methods ranging from detailed ground surveys to analyses of aerial and satellite imagery. Extension of optical remote sensing techniques to much larger, i.e., continental, scales can be frustrated by the inherent limitations of cloud-cover. Due to the strong positive correlations between vegetative cover, net precipitation and cloud-cover and self-reinforcing feedback loops, those regions of the planet most readily observed by optical techniques also tend to be the least vegetated. As a consequence, the actual distributions of vegetative types at continental to global scales is poorly known and studies requiring such information often rely upon maps of potential, pre-settlement, vegetation predicted on the basis of climate and physiography.

Land/atmosphere processes are governed by the type of land-cover and its quantity per unit area. Biomass, net quantity of biotic material per unit area, consists of living and dead fractions temporarily stored in both above and below ground pools. The sizes and distributions of these pools play a major role in the Earth's carbon cycle, yet the actual distribution of biomass is poorly known. In addition, the apportionment of living biomass between woody structural components and foliage determines the carbon fluxes required by maintenance and growth [2]. Destructive sampling for estimation of biomass is very difficult even for the aboveground fraction. As a consequence, biotic populations are often undersampled, and accurate estimates are elusive even at local scales. In spite of these difficulties, it is not uncommon for these local estimates to be applied as constants across biomes defined on the basis of potential vegetation maps in order to initialize surface conditions for global-scale models.

The atmosphere is nearly transparent to synthetic aperture radar. Thus, if land-cover classes are sufficiently distinctive with respect to their intrinsic structural and dielectric properties, then SAR data should be suitable for terrain classification and thereby compliment existing capabilities using optical sensors. The microwave dielectric constant is well known to be dependent upon the moisture content and dry density of biotic materials. Because microwave extinction losses through vegetation scale with frequency, there is a unique capability for radar to penetrate the canopy and directly sense the woody biomass fraction beneath the foliage. Multifrequency techniques can be used to "profile" the vegetative layer and provide information on both the foliar and woody biomass. However, microwave scattering is well known to be dependent upon the geometric properties of size, shape and orientation of the scattering elements, thus the relationships between radar backscatter and biomass can be expected to be nonunique and

Manuscript received March 7, 1995. This work was supported in part by the Jet Propulsion Laboratory under contract NASA-JPL-958438 and in part from the German Academic Exchange Service

M. C. Dobson, F. T. Ulaby, L. E. Pierce, K. M. Bergen, J. Kellndorfer, J. R. Kendra, E. Li, Y. C. Lin, A. Nashashibi, K. Sarabandi, and P. Siqueira are with the Radiation Laboratory, Department of Electrical Engineering and Computer Science, University of Michigan, Ann Arbor, MI 48109-2122 USA.

T. L. Sharik is with the Department of Forest Resources, Utah State Univ., Logan, UT 84322 USA.

IEEE Log Number 9412880.

dependent upon vegetation structural attributes. The purpose of this paper is to show how multifrequency, polarimetric SIR-C/X-SAR data can be exploited to yield more accurate estimates of various forest biophysical properties such as crown-layer biomass (foliage plus branches), tree height and basal area (net trunk cross-sectional area per unit ground area). These estimates are inputs to a simple biophysical model that uses common allometric relationships to yield estimates of trunk biomass and net aboveground standing biomass.

The overall objectives of this study are to develop and demonstrate a methodology for retrieval of forest biophysical properties based on radar backscattering behavior. Since structural attributes play such a critical role in determining backscattering behavior, a test site has been carefully selected to include plant communities with a range of distinctive architectures. The Raco Supersite is located at the southern ecotone of the boreal forest along a physiographic gradient of soil type, topography and moisture availability resulting from Wisconsinan glaciation of the Pleistocene Epoch (until 10 000 bp). Its lacrustine deposits, sandy glacial outwash plains and moraines support broad landscape patches of vegetation communities representative of both the boreal forest and the northern temperate forest. Thus, the results of this study may be more widely applicable over the natural ranges of the species considered.

A. Background

Two sets of factors exert primary control over radar backscattering from terrain: 1) geometric factors related to the structural attributes of the surface and overlying vegetation cover, and 2) dielectric properties mainly controlled by the relative moisture contents of the vegetation and underlying surface. Both sets of factors may be time-variant. Because of the resonance of water in the microwave region, the dielectric properties control the magnitude and relative phase of backscatter as a function of wavelength. Backscatter is proportional to volumetric moisture content within some scattering volume. To the extent that biotic materials are moist, this results in a correlation between backscatter and wet biomass.

Structural attributes also exert control over the frequency, polarization, relative phase and angular dependence of radar backscatter. In general, the total dynamic range in backscatter related to structural attributes is greater than that related to the natural variance in moisture-governed attributes. Within a resolution cell, the structural attributes of importance are known to be the plant architecture (size, shape and orientation of the woody stems); leaf size, shape and orientation; and surface roughness. The influence of each of these attributes on radar backscattering has been largely explored via theoretical modeling and empirical investigations using airborne and spaceborne SAR [3]–[14]. These studies present a strong case that structural properties are the primary determinants of radar backscatter and must be accounted for prior to determination of biomass related quantities. The variance of structural attributes over spatial scales greater than a resolution element imparts texture to radar imagery which is separable from the variance induced by coherent fading [15]–[18]. As a consequence, higher order statistical moments may contain information related to community structure (i.e., the presence of gaps) [19].

Image classification discriminates classes on the basis of features extracted from the spectral, spatial, or temporal domains. Two general approaches have been used to classify SAR imagery: 1) maximum likelihood classifiers, including both supervised and unsupervised cluster analysis and 2) knowledge-based techniques such as hierarchical decision trees and those based upon determination of dominant scattering mechanisms from electromagnetic theory. A key issue for any of these approaches is how consistent or stable the classifier is when applied to new regions or the same region at different times. Most recent classification efforts have used supervised maximum likelihood approaches; these often lead to very high classification accuracies for a given scene [20]–[28]. A given local region will only contain a subset of the terrain conditions existent within the full natural domain; hence, the extendability of locally-trained and supervised statistical classifiers can be impaired by the need for *a priori* information on probability of occurrence or for extensive local training populations. The knowledge-based techniques may overcome this limitation by first classifying on the basis of explicit relationships between radar backscatter and structural attributes [29]–[32]. These structural classes are then relabeled locally on the basis of known linkages between structure and floristic community. At present, such classifiers have been successfully tested locally, but have not yet been tested beyond the geographic province of their development.

An understanding of the causative factors for radar backscattering from forests has evolved through development of theoretical scattering models generally using a radiative transfer approach [3]–[17]. The model results are largely congruent with empirical data [33]–[45], and show the observed dependencies upon biomass and time-variant quantities such as changing dielectric properties. Most studies have concentrated on a single tree structural type (i.e., mono-species). Both models and data show that, for a given species (structural type), the radar backscattering coefficient ($\sigma^{\circ}_{f,p,\theta}$ at frequency band f, polarization p and incident angle θ) increases with biomass in a power-law relationship. Backscatter is shown to saturate at a biomass level that scales with wavelength for a given species. The hv- and hh-polarized backscatter are found to be the most sensitive to total biomass and hence yield the highest correlations; vv-polarized backscatter is more sensitive to crown-layer attributes and hence tends to saturate at lower levels of total biomass.

On this basis, some investigators have concluded that these saturation points define the upper limits for accurate estimation of forest biomass [44], [46]. This indeed is the case when only single frequency and polarization data are available. Importantly, when structurally dissimilar species are compared, both models and data show that there is structural control over both the slope of the power-law relationships and the saturation level at a given frequency and polarization. This is most evident when comparing the backscattering behaviors of different species [9], [31]. As a consequence, there is added information in the frequency and polarization behavior that can be brought to bear on the biomass estimation problem.

Models and some empirical data have shown that polarization ratios and spectral gradients do not saturate as quickly and can therefore be used to extend the range of biomass estimation beyond that imposed by the "apparent" saturation of a single frequency/polarization configuration [36], [42], [44]. "Apparent" is used here because backscatter often begins to decrease after biomass exceeds some structurally determined threshold; this decrease or darkening is related to increasing extinction of the signal. This effect can be seen in some of the empirical data reported in the literature [36], [40], [42], [45]. As a consequence, some studies have concluded that such ratios can be used to minimize species-related structural effects when defining power-law form estimation equations for total biomass. The spectral gradient of hv-polarized backscatter ($\sigma^{\circ}_{P,hv}/\sigma^{\circ}_{C,hv}$) was found to be best for this purpose in a study of forests in Maine using polarimetric AIRSAR data (P-, L- and C-bands) [42]. However, our experience with both AIRSAR and SIR-C data from the Raco Supersite indicates that such approaches are too simplistic and do not adequately account for structural effects of different species although they can extend the range of the estimates to higher levels of biomass within a given forest structural type.

In addition, most empirical investigations of mono-species forest stands show that there exists considerable scatter about the power-law relationship between backscatter and net biomass. However, model results indicate that much of this scatter is also a consequence of structural control, is therefore to be expected, and does not necessarily pose a limitation to accurate estimation of forest biomass [9], [47]. This can be understood by consideration of the following. In mature forests, most of the net biomass is contained within the woody main stems (often more than 90% of the total). Thus, to first approximation, biomass is the product of tree height, tree cross-sectional area, a taper factor and wood density as integrated over the stocking density of a given forest stand. For example, a few large and widely scattered trees can result in the same net biomass as many small but tightly packed trees; but the implications for radar backscattering are significantly different in the two cases. While such a situation may be infrequent for natural forests, many forests are managed. Management practices such as thinning, selective harvest, or leaving a few mature trees standing as seed sources after harvest can cause this situation to be quite common as is found in our data. Below saturation, the scattering models show that trunk height, basal area and stocking density have very different nonlinear effects on σ°. When the trunks are considered as near-vertical dielectric cylinders on a rough surface, σ° resulting from multiple, specular scattering from the ground and the trunks tends to vary linearly with stocking density and tree diameter and to vary with height squared. Consequently, in the example the net backscatter from the few tall trees will be much greater than that from the many small trees of equivalent net biomass. As a result, attempts to estimate net biomass directly from a simple power-law function of σ° cannot account for this sort of structurally induced scatter in the relationship.

An argument has been recently presented that this apparent "noise" in the simple power-law relationship of σ° with total biomass is additional "signal" that can be exploited to improve the accuracy of biomass estimates [9]. The key to exploiting this "signal" is to estimate net biomass indirectly through a three-step process. First, the primary structural attributes (i.e., basal area, height and crown biomass) are estimated from SAR data for a given structural type. Then the trunk biomass is estimated as the product of basal area, height, a main stem taper factor and the dry density of the main stem. Finally, the net biomass is determined by the sum of the SAR-derived crown biomass and the trunk biomass. This approach was partly explored via a neural network technique and found to yield very satisfactory results [47]. The three-step approach is further developed in this paper.

B. Methodology

Assuming *a priori* classification of land-cover, empirical formulations are developed herein and used to estimate forest biophysical properties from multifrequency and polarimetric radar backscatter. Distinctive formulations are used for each structural class. Locally defined allometric relationships between tree diameter and height are used in conjunction with measurements of wood density in order to estimate trunk biomass from SAR-derived estimates of tree height and basal area.

The *a priori* classification can be based on the SAR data itself or from some other source. SIR-C/X-SAR data acquired during SRL-1 in April 1994 at the Raco Supersite have previously been classified into terrain classes [32]. This classification uses a hierarchical approach to discriminate structural classes. At each step, a knowledge-based conceptual model derived from theoretical modeling and antecedent measurements is used to select discriminant features on the basis of simple structural attributes such as branching architecture and foliage shape and size. The classification results are evaluated for an independent testing population. A key is used to translate the structural categories into the names of local floristic types. These classification results are summarized in Table I. In this study we assume 100% correct classification in order to decouple errors in the the biophysical retrievals from those in classification.

II. Site Description

The Raco Supersite investigated during the SIR-C/X-SAR missions is at the eastern end of the Upper Peninsula of Michigan (Fig. 1). Its center coordinates are 46°15′ N. latitude and 84°30′ W. longitude. Located at the ecotone between the boreal forests and northern temperate forests, this transitional zone is expected to be ecologically sensitive to anticipated global changes resulting from climatic warming. Baseline studies of vegetation communities are essential to future monitoring of such changes.

This site contains most boreal forest species as well as many of the temperate species, thus studies here serve to link studies performed well to the north and south. The distribution of forest communities is largely determined by a soil-controlled resource gradient established by glacial deposits such as moraines and outwash. Typically, landscape patch sizes are large; homogeneous forest stands usually

TABLE I

			PERCENT CLASSIFIED AS (Independent Test Region)					
	Structural Class	Type	Tall Vegetation				Short Vegetation	Surface
		Tree Form	Excurrent		Decurrent		NA	NA
		Branch Size	Large	Small	Large	Small		
		Foliage Type	Long Needle	Short Needle	None	None		
	Local Floristic Community		Upland Conifers	Lowland Conifers	Northern Hardwood	Aspen & Birch	Grasses, Sedges, Shrubs	Bare Soil, Paved, Water
TRUE CLASS	Upland Conifers		94.53	0.01	5.38	0	0.08	0
	Lowland Conifers		4.53	92.88	2.41	0.11	0.07	0
	Northern Hardwood		0.87	7.81	90.30	1.02	0	0
	Aspen & Birch		0	5.49	6.11	88.40	0	0
	Short Vegetation		0.85	0.01	1.41	0.02	96.38	1.33
	Surface		0	0	0	0	1.05	98.95

Average Classification Accuracy: 94%

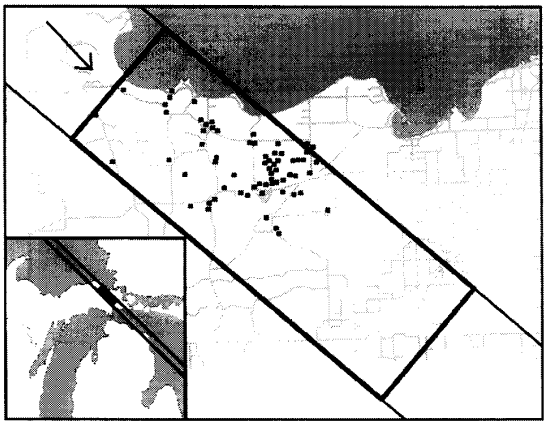

Fig. 1. Map of Raco Supersite location. Inset depicts path of orbit 102 over Michigan and the Great Lakes. Detail shows area of scene 102.41 and permanent forest test stands.

exceed 10 ha in size. Represented communities include: 1) northern hardwoods: sugar maple (*Acer saccharum*), red maple (*Acer rubrum*), American beech (*Fagus grandifolia*), eastern hemlock (*Tsuga canadensis*) and balsam fir (*Abies balsamea*); 2) upland pine communities: jack pine (*Pinus banksiana*), red pine (*Pinus resinosa*) and eastern white pine (*Pinus strobus*); 3) lowland conifer bogs: black spruce (*Picea mariana*), white spruce (*Picea glauca*), northern white-cedar (*Thuja occidentalis*) and tamarack (*Larix laricina*); 4) lowland hardwoods: red maple, white birch (*Betula papyrifera*), yellow birch (*Betula alleghaniensis*) and trembling aspen (*Populus tremuloides*); and 5) areas of disturbance induced pioneer species: trembling aspen, bigtooth aspen (*Populus grandidentata*), cherries (*Prunus pensylvanica*, *Prunus serotina* and *Prunus viginiana*) and serviceberry (*Amelanchier*). The site is not totally forested. Scattered permanent clearings, hayfields and a large agricultural region in the southeastern portion of the site provide areas of relatively low biomass and variable surface roughness conditions. The Michigan Department of Natural Resources inferred the distribution of these community types from high altitude aerial photography obtained in 1979 (Fig. 2).

Fig. 2. Land-cover distribution at Raco Supersite as inferred by the Michigan department of natural resources from high altitude aerial photography obtained in 1979.

Importantly, the forest species at the Raco Supersite represent two major branching architectures (excurrent and decurrent tree forms) and leaf types (broadleaf and needle-leaf). The excurrent branching pattern is a result of the central stem

outgrowing the lateral branches; this results in a cone-shaped crown and a cylinder-shaped central trunk. Most coniferous species are excurrent. The decurrent branching pattern arises when the lateral branches grow as fast or faster than the main stem; the definition of a central trunk can be completely lost due to repeated forking. Most dicotyledonous trees are decurrent in form as adults [48]. Some deciduous species modify form with age; at the Raco Supersite young aspens are excurrent and undergo transition to a decurrent form with maturity.

A stratified sample of each of the dominant forest communities were selected for biometric survey. This sample population consists of over 60 stands. A 200 m by 200 m sample area was surveyed within each stand and located at least twice the height of the trees from all stand edges. The coordinates of the corners were obtained using GPS with 3-D differential processing and are generally accurate to within 10 m. The sampling strategy applied to each sample area was designed to yield a 15% (or better) uncertainty about the measured means at a 95% confidence level. Within each 4 ha sample area, 40 sampling points were located along 5 transects using systematic sampling with a random start. At each sampling point, a set of nested circular plots of area 100 m^2, 32 m^2 and 3 m^2 were established to characterize the upper stratum (height > 5 m), middle stratum (1 m $<$ height $<$ 5 m) and the lower stratum (height < 1 m), respectively. The diameters of all live and dead stems were recorded by species to the nearest 0.1 cm. For the upper stratum, the diameters were measured at breast height (1.37 m); basal diameters (15 cm above the ground) were recorded for middle stratum stems. Within each plot, a subsample of the stems was measured for total height and height to the lowest live branch using clinometers and height poles. The difference is the crown thickness. This subsample was used to generate stand specific allometric equations to estimate height from diameter for each species. These equations take the form of second-order polynomials [49], [50].

Allometric regression equations developed by other investigators [51]–[60] were used to estimate dry biomass of tree components (main stem, branches and foliage) on a per tree basis for each live stem. Often, there are separate sets of expressions for small and large trees. Within each of the sample plots, the tree-level biomass estimates were summed over the sampled area and expressed in terms of kg/m^2. Crown biomass is the sum of branch and foliage biomass. Basal area is calculated as the sum of measured stem cross-sectional area per unit area of ground. Stocking density is the number of stems per unit area.

Biometric surveys at the Raco Supersite were conducted in 1991 (14 stands), 1992 (16 stands), 1993 (33 stands) and 1994 (reinventory of the youngest 26 stands). The sampling design inventoried all stems within 10% and 3.2% of the 4 ha plot area for the upper and middle strata, respectively. Previous application of this sample design to similar forest stands indicated that the average expected uncertainty about the measured means should be on the order of 15%. The actual sampling error was evaluated through an analysis of the with-in stand variance (among the 40 sampling locations) of the biometric data obtained in 1991 and 1992. Over these 30 stands, the average uncertainty around the measured means is calculated to be 14.1%, 16% and 21.9% for diameter, basal area and stocking density, respectively, at the 0.05 significance level. The uncertainties are found to be highest for young conifer seedlings and least for mature conifer plantations and northern hardwoods. An overview of the mean biophysical characteristics is shown in Fig. 3; stocking density, basal area, height and net aboveground dry biomass are presented relative to mean stem diameter.

III. Site Characteristics and Data Acquisition

The Raco Supersite was imaged 12 times from Apr. 9–19 during the SRL-1 mission. Over this period, data were acquired on both ascending and descending nodes of the orbit with SAR look angles ranging from 19° to 47° relative to nadir. The data acquired on Apr. 15, 1994 during the descending portion of orbit 102 at a look angle of 31° are used in this report. This scene was selected for two reasons. First, five of the SRL-1 data acquisitions over the Raco Supersite have look angles within ±5° of this scene and most are for descending passes of the shuttle. Thus, this scene is highly representative of the average SAR imaging parameters used during SRL-1. The second consideration relates to ground conditions at the Raco Supersite. Apr. is a time of great dynamic change in surface properties and vegetation conditions. On the day of launch, Whitefish Bay on Lake Superior was completely ice-covered as were all inland lakes; snow-cover was 100% and snow-depths range from 50 cm in lowland conifer stands adjacent to Lake Superior to 20 cm in forest clearings. By Apr. 19, the ice-pack on Lake Superior had broken and shifted; warm daytime temperatures reduced snow-cover to zero in clearings and less than 30 cm in heavily forested areas. Most of the change had occurred prior to Apr. 15. Thus, this scene is also largely representative of site conditions during the last 3/4 of the SIR-C/X-SAR data acquisitions over the Raco Supersite during SRL-1.

A. SIR-C/X-SAR Data

A summary of the SIR-C/X-SAR imaging parameters is given in Table II for the descending scene acquired during data-take 102.41. The fully polarimetric SIR-C data at L- and C-bands (vv-polarized X-SAR data at X-band) were processed by the Jet Propulsion Laboratory (Deutsche Forschungsanstalt für Luft- und Raumfahrt) to single-look complex values in slant range format. Calibration values for antenna pattern correction and amplitude and phase correction are those provided by JPL and DLR. No further calibration is applied to these standard SAR image products although the Raco Supersite was instrumented with an array of passive and active calibration targets as well as a polarimetric scatterometer used to define the average Mueller matrix of distributed targets. A comparison of the standard JPL calibration factors with those derived from local point and distributed targets is discussed in [61]. Within the context of this paper, absolute calibration errors are not of great concern, provided that they do not vary across the image swath in the range direction. However,

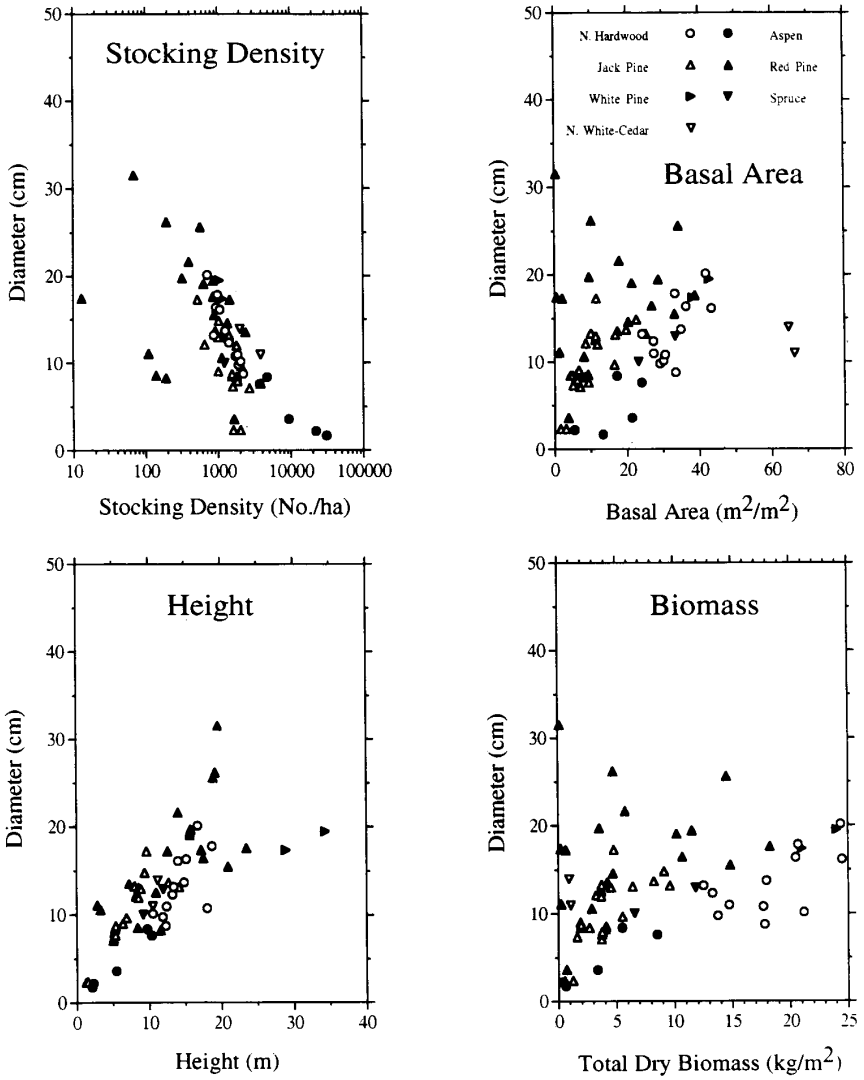

Fig. 3. Overview of average forest biophysical characteristics determined by biometric surveys.

such errors are of concern with respect to applying the algorithms developed herein to other scenes at this or other sites. Calibration errors, if determined, for SIR-C/ X-SAR data will establish a series of linear offsets that must be applied to the biophysical estimation algorithms presented in Section IV.

The SIR-C/X-SAR imagery for this scene is shown in Fig. 4 for L- and C-bands as three-polarization (hh, vv, hv) false-color composites and as a multifrequency (L-, C-, and X-band) composite. Histogram equalization stretches are separately applied to linear received power for each channel in Fig. 4. Ground control points were used to coregister X-band to the SIR-C (L- and C-band) data. A second-order polynomial warp is used for coordinate transformation, and yields offset errors less than 25 m. In order to segment and extract SAR data from known regions of interest, a geographic information system containing land-cover (Fig. 2), soils, digital

TABLE II

Mission: SRL-1 Orbit: 102 Data-Take: 102.41
Date: April 15, 1994 Time: 17:00:31.723 (GMT)

Sensor Parameters			
Band	L	C	X
Frequency (GH_z)	1.25	5.3	9.6
Wavelength (cm)	24	5.66	3.125
Polarizations	polarimetric		v v
Pulse Bandwidth (MH_z)	20		19
PRF (H_z)	1620		1620
Image Parameters (single look, slant range)			
Image Center (lat., long.)	46.37°N, 84.89°W		46.39°N, 85.0°W
Look Angle (near - far range)	30.3°- 33.8°		29.6° - 33.1°
Pixel Spacing (range/azimuth)	6.66m/4.48m		6.66m/4.49m
Pixel Resolution (range/azimuth)	7.4m/6.2m		7.33m/6.3m
Post Processing (avg. Mueller Matrix)			
Pixels Averaged (range/azimuth)	2/6		2/5
Pixel Spacing at Center (ground range/az.)	24.9m/26.9m		25.5m/22.5m
Number of Looks	7.7		6.5

elevation and the location of surveyed forest stands (Fig. 1) is transformed into slant range and then coregistered to the composite multifrequency SAR imagery. The coregistration accuracy is also estimated to be on the order of $+/-25$ m. Post processing of the data included averaging using a 5×5

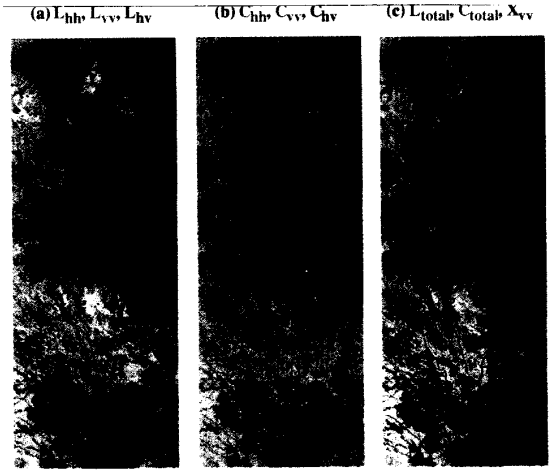

Fig. 4. SIR-C/X-SAR image of Raco Supersite acquired during orbit 102 on Apr. 15, 1994: (a) L-band, (b) C-band and (c) L/C/X-bands. For single frequency images, red = hh, green = vv and blue = hv. For multifrequency image, red = L-band, green = C-band and blue = X-band; L- and C-bands are total power. A linear enhancement has been applied to all channels.

window for σ° and determination of the peak co-polarized relative phase difference at L-band (L_ζ) and C-band (C_ζ) from the average Mueller matrix [62].

B. Site Characteristics

The week preceding this overpass by SIR-C/X-SAR was characterized by a warming trend with min./max. temperatures increasing from −11.7/8.9°C to 1.1/12.8°C on Apr. 15 [63]. The air temperature at the time of this data-take was 10°C. As a consequence, tree borings for temperature and dielectric measurements showed all trees to be completely thawed aboveground. A light rain fell prior to the overpass; 0.86 cm of precipitation was recorded at the Raco airfield during the period from 05:00 to 09:00. The precipitation was associated with somewhat scattered thundershowers. A network of 21 rain gauges distributed across the test site recorded an average rainfall of 1.26 cm over a 24-hour period. The precipitation was not uniformly distributed; amounts tended to be lowest along Lake Superior and greatest in the vicinity of the Raco Plain.

Whitefish Bay in Lake Superior appears in the upper right corners of the images in Fig. 4. At the bottom of the image is a 20 km × 20 km agricultural region of hayfields on drained lacrustine deposits; the characteristic pattern is due to variable roughnesses and dormant vegetation covers on the snow-free, but saturated soils. Above the agricultural area is a poorly drained region of spruce-dominated lowland conifer bogs; these regions produce relatively high return at all frequencies and polarizations and thus appear very bright in Fig. 4. Snow-cover is still relatively deep in similar northern white-cedar bogs along the Lake Superior shore (32 cm average snow depth). Beneath the snow, the surface is saturated with water; gravimetric moistures of the organic horizon can exceed 3000% on a dry weight basis.

Above these lowland conifers in the center of Fig. 4, the elevation rises by approximately 20 m to an excessively drained sandy outwash plain known as the Raco Plain. This area contains scattered clearings and is dominated by upland conifer stands (red pine and jack pine) that appear pink in Fig. 4(a) due to strong backscattering at $\sigma^\circ_{L,hh}$. The black triangular feature is due to 1.5 km runways at the decommissioned Raco airbase. The two major types of upland conifers are differentiated by multifrequency data; all stands of red pines appear as red in Fig. 4(c) while jack pines appear more green. Average snow depth ranges from 7–25 cm in red pine stands and was found to average 23 cm on Apr. 16–17. The upper 10 cm of all soils on the Raco Plain are thawed and are wet to saturated with water; average gravimetric moistures vary from 15% to 30% in clearings and from 60% to over 400% in upland forest stands.

In the upper left of Fig. 4 are areas of high return (spruce-dominated lowland conifer bogs) and scattered plantations of red pine. To the right of these lowlands (upper middle of Fig. 4) is a terminal moraine that roughly parallels the Lake Superior shore. The moraine is dominated by scattered aspen stands in successional sequence to northern hardwood communities. The relatively high cross-polarized return of the excurrent northern hardwoods and mature aspens causes this region to appear darker and bluish in Fig. 4. Local depressions in the moraine are filled by scattered inland lakes; these are ice- and snow-covered. Snow-cover is still continuous within these leafless deciduous forest stands on Apr. 17; snow depth averages 25 cm. Gravimetric soil moisture ranges from 70% to 1,000% in the saturated upper 5 cm of the organic and mineral soil horizons. Aspens, birch and lowland conifer communities generally line the shore of Lake Superior.

IV. Estimation of Forest Biophysical Properties

The SIR-C/X-SAR data (Fig. 4) was segmented for the forest test stands (Fig. 1). The mean backscattering coefficient σ° for each of the three linear polarization combinations (hh, hv and vv) are plotted versus basal area, average tree height and total aboveground dry biomass in Fig. 5 at both L- and C-bands. For a given frequency and polarization, σ° is found to have a power-law relation to the biophysical variate; however, there is much scatter in the data. In addition, σ° is found to increase at very low levels of dry biomass (i.e., <1 kg/m^2) due to sensitivity to surface properties such as roughness and moisture as forest biomass becomes negligible.

Other studies have sought to find indices using σ° and relative phase differences to minimize the scatter observed in Fig. 5; and thus permit use of a singular expression for estimation of dry biomass that is independent of forest structural differences. One such index is the ratio of long to short wavelength cross-polarized backscatter [42]. The $\sigma^\circ_{L,hv}/\sigma^\circ_{C,hv}$ ratio is calculated for the various forest stands in this study (Fig. 6). In general, $\sigma^\circ_{L,hv} < \sigma^\circ_{C,hv}$ at low biomass and $\sigma^\circ_{L,hv} > \sigma^\circ_{C,hv}$ at high forest biomass for a given forest community. Although this ratio is found to be generally well-behaved within a forest structural type, it is obvious that this relatively simple approach does not compensate for all of the structural effects. As a result, the generalized least-squares power-law fit to the data yields a low correlation ($r^2 = 0.22$)

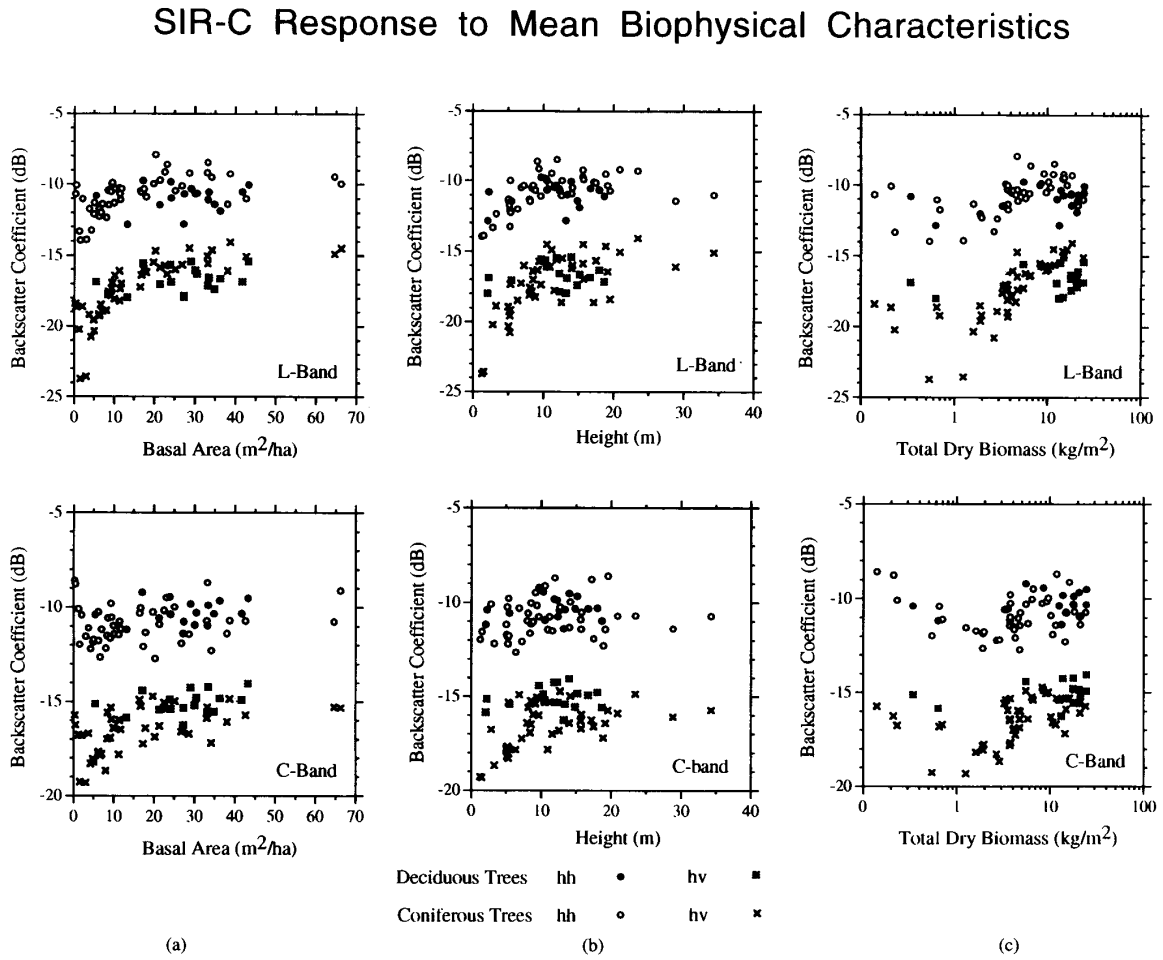

Fig. 5. Radar backscatter versus mean forest biophysical characteristics: (a) basal area, (b) height and (c) total dry biomass.

of total dry biomass with $\sigma^{\circ}_{\mathrm{L,hv}}/\sigma^{\circ}_{\mathrm{C,hv}}$ when calculated over the entire sample population. Tests of other simple indices did not perform significantly better at reducing the scatter related to forest structural types.

If structural effects on σ° cannot be ignored, then a different approach must be taken that explicitly accounts for these effects. This section presents one such approach based upon a simple biophysical model with empirically driven coefficients that account for allometric relationships, moisture conditions and wood density. The approach assumes that forest structural types are either known *a priori* or estimated via classification with the SAR data itself. The results in Table I show that such a classification can be performed with good accuracy.

A. Model

A simple biophysical model of aboveground standing biomass in a forest is given by

$$B_d = B_c + B_t \tag{1}$$

where

B_d = total dry standing biomass (kg/m^2)
B_c = dry biomass of crown (kg/m^2)
B_t = dry biomass of trunks (kg/m^2).

The crown biomass consists of both the foliage and small woody stems. For a single tree with a tapered, cylindrical trunk, the trunk volume V_t can be determined geometrically as

$$V_t = \frac{\pi h d^2 t}{4} \tag{2}$$

where

h = trunk height
d = trunk diameter
t = trunk taper factor.

The dry biomass of a single trunk b_t is then the product of V_t and the dry density of wood ρ_s. Hence,

$$b_t = \frac{\pi h d^2 t \rho_s}{4}. \tag{3}$$

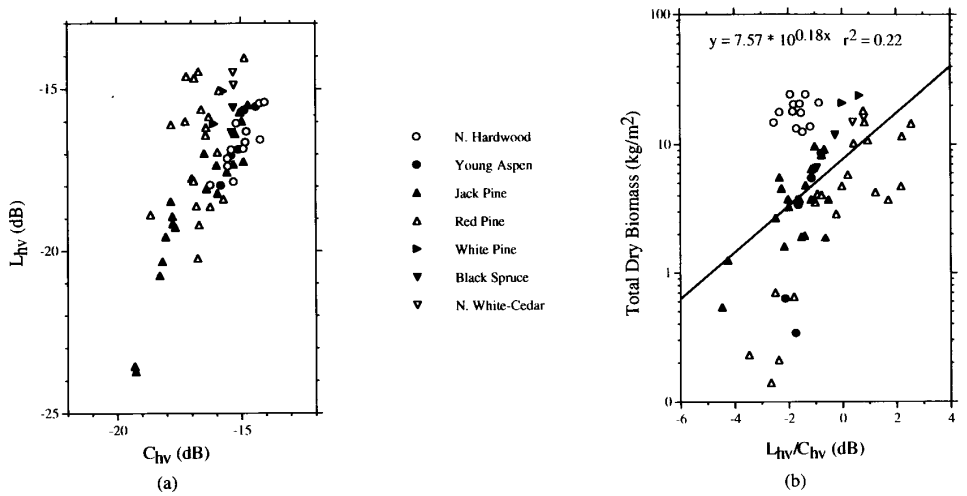

Fig. 6. Effectiveness of cross-polarized ratios for reducing structural effects on direct estimation of total dry biomass: (a) L_{hv} vs. C_{hv} and (b) L_{hv}/C_{hv} (dB) vs. total biomass.

Calculation of trunk biomass on a stand basis is performed by summation of b_t over the distributions of height and diameter within stocking density S

$$B_t = \sum_{j=1}^{S} \frac{\pi h_j d_j^2 t \rho_s}{4}. \tag{4}$$

For the SIR-C/X-SAR data, the single look resolution area is approximately 46 m^2 (Table II). σ° is generally calculated as an average over a much larger N of looks (i.e., $N > 30$). Hence, σ° represents an ensemble average over a relatively large area (75 m $\times$ 75 m in this study), and consequently contains many individual trees. If all trees within this area have identical heights and diameters, then B_t can be expressed in terms of the basal area b_a as

$$B_t = \rho_s t h b_a \tag{5}$$

where $b_a = \pi d^2 S/4$. However, forest stands contain a great deal of variance in h and d and often include multi-modal distributions related to mixed species and age distributions of stems. In addition, h, d and S are not independent random variates, hence the product of average height, basal area and taper factor do not generally yield the average biomass. As a consequence, it is more appropriate to use an approximate form of (5)

$$B_t \approx \rho_s t_s \bar{h} b_a \tag{6}$$

where t_s is an effective taper factor for a given structural type and $\bar{h}$ is the average tree height.

For many forest species allometric equations have been determined to relate height to diameter and these variates to biomass. If height and diameter were perfectly correlated for a given species, then (3) and (4) could be uniquely determined given only height or diameter. This, however, is not the case; hence both height and diameter distributions need to be measured to accurately estimate stand biomass. In addition, competition, natural disturbance processes and silvicultural management modify stocking density over time. As a result, B_t does not necessarily vary in a monotonic fashion with either h or d. Within a given region, it is not uncommon to find stands of a given species composition with equivalent biomass but very different distributions of h, b_a and stocking density S.

The net backscatter σ° from a forest can be modeled by

$$\sigma^\circ = \sigma_c^\circ + \tau_c^2 \tau_t^2 (\sigma_t^\circ + \sigma_s^\circ + \sigma_{st}^\circ) \tag{7}$$

where

σ_c° = backscatter coefficient of the crown layer of smaller woody branches and foliage
τ_c = transmissivity of the crown layer
τ_t = transmissivity of the trunk layer
σ_t° = backscatter coefficient of the trunk layer
σ_s° = backscatter coefficient of the surface
σ_{st}° = backscatter coefficient resulting from interaction of the surface and the trunk layer.

Radiative transfer approaches have been used to model the backscattering coefficients and transmissivities of the various layers given in (7) for a number of forest types [3]–[17]. When model calculations are depicted versus the net dry biomass for a given forest structural type they display characteristic behaviors of the form exhibited by empirical data. Several aspects of these characteristic behaviors are illustrated in Fig. 7(a) which shows polynomial fits of dry biomass to $\sigma_{L,\mathrm{hv}}^\circ$ observed by SIR-C. First, the relationships tend to be distinctive for each forest structural type. Secondly, there are three general regions within each characteristic curve: 1) a region of very low dry biomass, 2) a region of moderate biomass and c) a region of high biomass. In the low biomass region, σ° is dominated by σ_s° since σ_c°, σ_t° and σ_{st}° are small and τ is close to 1.0. In the moderate biomass region, σ° is roughly proportional to biomass and is dominated by σ_c°, σ_t°, and σ_{st}°; and τ is reduced sufficiently to limit the relative

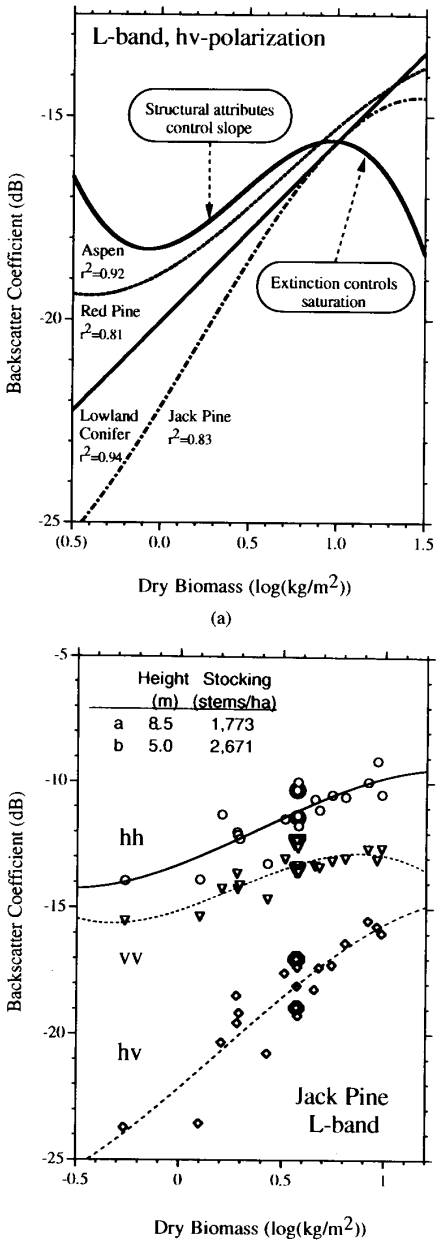

Fig. 7. Forest structural attributes control (a) the slope and saturation level of the power-law relationship of biomass to $\sigma^\circ_{f,PP}$ and (b) the scatter about this relationship within a given forest structural type. The data for two stands of equivalent biomass are in bold symbols; at each polarization σ° for stand (a) is largest.

contribution of σ°_s. In the high biomass region, or zone of saturation, τ_c and/or τ_t have become small enough to cause extinction losses to exceed incremental increases in σ°_c, σ°_t and σ°_{st} as biomass is increased. As a result, σ° saturates and may decrease as net biomass increases beyond some threshold.

The scattering models tell us that there is structural control of the behavior in all three regions. In the low biomass region, σ° is sensitive to surface roughness. In the saturation region, extinction is determined by the sizes of the scattering elements (woody cylinders and foliage) relative to wavelength and their packing density. At sufficient packing density or vertical thickness, the crown layer can become opaque and block scattering contributions from larger woody elements below, thus causing net σ° to decrease (darkening effect). The slope of the relationship in the moderate biomass region is determined by structural attributes of the vegetation such as the sizes of scattering objects relative to wavelength (length and diameters of cylindrical woody stems) and the numbers of such objects per unit area. The orientation distributions of the scatterers determine the polarization behaviors of the scattered fields at a given wavelength. Hence, within this region σ° is primarily determined by forest architecture: the height distributions of trees, species-dependent allometric relationships (height to diameter relationships), and stocking density. The power-law behavior in this region is that expected for backscatter and bistatic scattering involving woody dielectric cylinders.

For example, the bistatic radar cross section of a perfectly conducting cyliner in the specular direction is given by [64]

$$\sigma_{\text{cylinder}} = kdh^2 \cos\left(\frac{\pi}{2} - \theta\right) \tag{8}$$

where θ is the angle of incidence relative to the axis of the vertical cylinder. The backscatter at broadside to such a cylinder is kdh^2. Of course trees are not perfectly conducting, and the effects of wood as a lossy dielectric are only approximated by

$$\sigma_{st} \approx \Gamma_t \Gamma_s e^{-(2k\sigma\cos\theta)^2} kdh^2 \cos\left(\frac{\pi}{2} - \theta\right) \tag{9}$$

where

Γ = Fresnel reflection coefficient in the specular direction for the woody cylinder (Γ_t) and the ground surface (Γ_s)
d = diameter of woody cylinder
h = height or length of cylinder
k = wavenumber
σ = rms roughness of the ground surface.

For a stocking density S of identical cylinders,

$$\sigma^\circ_{st} = S\sigma_{st}/A. \tag{10}$$

where A is the illuminated area. Thus, in forest communities where height, diameter and stocking density are highly correlated, a power-law relationship is expected between σ° and B_t. Secondly, to the extent that h, d and S relationships are distinctive between species, then there will be species-related structural control of the slope of this power-law relationship as evidenced in Fig. 7(a).

Another implication of (7)–(10) is that scatter is expected about the characteristic power-law behavior for a given structural type. This is because σ° is proportional to sdh^2 while biomass is proportional to sd^2h. Thus, two stands of equivalent biomass can be expected to produce very different σ°. This effect is illustrated by the SIR-C data for jack pine forests in Fig. 7(b). Two stands are annotated; both having total dry

TABLE III

Structure		Local Species Name	Biophysical Variate	Units	Equation	No. of Cases	r^2	RMSE
Group	Sub-Group							
A. Using SIR-C Data Only								
Decurrent	All	N. Hardwoods	Height	m	$-0.498L_\varsigma + 8.387$	17	0.198	4.20
	(no leaves)	and	Basal Area	m^2/ha	$1.109C_\varsigma + 30.249$	17	0.389	7.43
		Aspen	Trunk Biomass	kg/m^2	$0.026\hat{h}\hat{b}_a + 2.676$	17	0.228	5.33
			Crown Biomass	kg/m^2	$0.169C_\varsigma + 2.966$	17	0.286	1.42
			Total Biomass	kg/m^2	$\hat{B}_c + \hat{B}_t$	17	0.249	6.59
Excurrent	All	Lowland	Height	m	$2{,}211.798 * 10^{\left(0.199\sigma^\circ_{L,vv}\right)} + 3.839$	46	0.397	6.00
		and	Basal Area	m^2/ha	$183.743 * 10^{-0.286\left(\sigma^\circ_{L,vv} - \sigma^\circ_{L,hv}\right)} + 4.948$	46	0.333	12.42
		Upland	Trunk Biomass	kg/m^2	$0.025\left(\hat{h}\,\hat{b}_a\right)^{1.021} - 1.215$	46	0.599	3.05
		Conifers	Crown Biomass	kg/m^2	$0.295\left(\sigma^\circ_{L,hv} - \sigma^\circ_{C,vv}\right) + 3.369$	46	0.531	0.68
			Total Biomass	kg/m^2	$\hat{B}_c + \hat{B}_t$	46	0.585	3.72
B. Using SIR-C/X-SAR Data								
Decurrent	All	N. Hardwoods	Height	m	$-4.344\left(\sigma^\circ_{L,hv} - \sigma^\circ_{X,vv}\right) - 4.712$	10	0.304	2.53
	(no leaves)	and Aspen	Trunk Biomass	kg/m^2	$0.043\,\hat{h}\hat{b}_a - 2.397$	10	0.419	3.72
Excurrent	All	All Conifers	Basal Area	m^2/ha	$23.656 * 10^{0.241\left(\sigma^\circ_{L,hv} - \sigma^\circ_{X,vv}\right)} + 7.808$	17	0.489	8.95
			Trunk Biomass	kg/m^2	$0.013\left(\hat{h}\,\hat{b}_a\right)^{1.021} + 0.663$	17	0.671	3.21

biomass of approximately 3.8 kg/m^2. Both plantation stands have similar surface conditions with respect to snow cover and surface roughness; however, at L-band, σ° can be as much as 2 dB different. As expected from (9) and (10), the taller trees with a smaller stocking density have larger σ°.

In summary, the effects of forest structure are found to yield ambiguities in the relationship of σ° to B_t. The ambiguities are caused by 1) structural differences in growth form and branching architecture, 2) between-stand differences in height, diameter and stocking density, and 3) saturation effects as the forest becomes more opaque at high levels of biomass. As a consequence, direct inversion of σ° for biomass can be ill-posed without explicit accounting for structural effects. In concept this could be done *via* inversion of the nonlinear scattering models, provided that polarimetric observations are available over a wide range of incidence angles. In practice, for a space-borne SAR, this is generally not realizable as only a single angle is available at any given time.

To overcome this dilemma, a three-step process is proposed. First, *a priori* information or classification of terrain using SAR data can be used to assign the forest structural type of a given region. Second, polarimetric SAR data is used to estimate the fundamental parameters in the simple biophysical model (height, basal area and crown biomass). The estimation equations are structure-specific to account empirically for tree form, branching architecture and foliage characteristics. Finally, trunk-layer biomass B_t is estimated from estimates of basal area ($\hat{b}_a$) and height ($\hat{h}$) using *a priori* knowledge of taper factor and wood density for a given structure type. Hence, the inversion model is given by

$$\hat{b}_{a_i} = f_{1_i}(\sigma^\circ) \tag{11}$$

$$\hat{h}_i = f_{2_i}(\sigma^\circ) \tag{12}$$

$$\hat{B}_{t_i} = \rho_{s_i} t_i \hat{b}_{a_i} \hat{h}_i + c_i \tag{13}$$

$$\hat{B}_{c_i} = f_{3_i}(\sigma^\circ) \tag{14}$$

$$\hat{B}_{d_i} = \hat{B}_{t_i} + \hat{B}_{c_i} \tag{15}$$

where the functions f_1, and f_2 and f_3 are empirically derived using least-squares techniques for the i structural type. The coefficients for (13) are empirically derived for each structural type using measured biometric data, allometric equations available in the literature and measurements of wood density.

B. Biophysical Estimation Using SIR-C Data Alone

The SIR-C data and the biometric data from the 63 forest test stands at the Raco Supersite are used to solve for the functions and coefficients in (11)–(14) for each forest community. A subset of the measured data is used in this process and includes only stands where $B_d > 2.5$ kg/m^2. This biomass filter minimizes the sensitivity of the solution to surface roughness effects and is consistent with the SAR-based terrain classification which distinguishes tall vegetation as being $\gtrsim$2.5 kg/m^2. Least-squares techniques are used to

TABLE IV

Structure		Local Species Name	Biophysical Variate	Units	Equation	No. of Cases	r^2	RMSE
Group	Sub-Group							
A. Using SIR-C Data Only								
Excurrent	Long	Upland	Height	m	$7{,}403.452 * 10^{\left(0.2389\sigma^{\circ}_{L,vv}\right)} + 3.075$	40	0.781	4.14
	Needles	Conifers	Basal Area	m^2/ha	$76.377 * 10^{0.174\left(\sigma^{\circ}_{L,hv} - \sigma^{\circ}_{C,hh}\right)} + 4.723$	40	0.594	6.23
			Trunk Biomass	kg/m^2	$0.013(\hat{h}\hat{b}_a)^{1.029} + 0.957$	40	0.545	2.55
			Crown Biomass	kg/m^2	$0.257(\sigma^{\circ}_{L,hv} - \sigma^{\circ}_{C,hh}) + 3.118$	40	0.561	0.65
			Total Biomass	kg/m^2	$\hat{B}_c + \hat{B}_t$	40	0.602	2.69
Excurrent	Short	Lowland	Height	m	$1.162(\sigma^{\circ}_{L,vv} - \sigma^{\circ}_{C,vv}) + 12.012$	4	0.630	0.62
	Needles	Conifers	Basal Area	m^2/ha	$-14.519(\sigma^{\circ}_{L,hh} - \sigma^{\circ}_{L,hv}) + 136.826$	4	0.951	4.21
			Trunk Biomass	kg/m^2	$0.135(\hat{h}\hat{b}_a)^{0.711} - 1.179$	4	0.958	0.61
			Crown Biomass	kg/m^2	$0.971\sigma^{\circ}_{L,hv} + 17.394$	4	0.990	0.07
			Total Biomass	kg/m^2	$\hat{B}_c + \hat{B}_t$	4	0.968	0.65
B. Using SIR-C/X-SAR Data								
Excurrent	Long	Upland	Basal Area	m^2/ha	$25.366 * 10^{0.244\left(\sigma^{\circ}_{L,hv} - \sigma^{\circ}_{X,vv}\right)} + 5.928$	16	0.640	7.25
	Needles	Conifers	Crown Biomass	kg/m^2	$0.432\left(\sigma^{\circ}_{L,hv} - \sigma^{\circ}_{X,vv}\right) + 2.928$	16	0.790	0.84

find solutions for f_1, f_2 and f_3 for each structural class having a statistically significant sample population. Simple linear functions of σ° and peak relative co-polarized phase difference ζ at L-band, L_ζ, and C-band, C_ζ, are selected on the basis of maximum correlation coefficient r^2.

Separate equation sets are derived for each of three *a priori* classification scenarios: 1) classification of trees only on the basis of tree form (only excurrent and decurrent forms exist at the Raco Supersite), 2) additional subclassification of excurrent trees on the basis of needle size (this distinguishes upland and lowland conifer communities at the Raco Supersite), and 3) further subclassification of both excurrent and decurrent tree forms on the basis of relative branch architecture (this yields categories congruent with the structural classes resulting from classification by SIR-C/X-SAR). The empirical retrieval equations for these three classification scenarios are given in Tables III-V, respectively. Although multiple linear solutions yield higher correlations, the improvement is generally marginal and hence are not presented in Tables III-V or used herein. Except where noted, σ° is in dB and ζ is in degrees in these tables. The values of correlation coefficient and rms error are those obtained by application of the estimation functions to all test stands of that structural class including those where $B_d < 2.5$ kg/m^2. In general the crown biomass function uses data at C-band alone or ratioed to σ° at L-band. The functions for $\hat{b}_a$ and $\hat{h}$ primarily make use of σ° at L-band and polarization ratios with the exception of the decurrent tree forms.

When considering the results obtained using classifications at the two finest levels (Tables IV and V), it is important to note that the results for lowland conifers are only based upon four stands (two white-cedar stands and two spruce stands). In addition, the results for the decurrent-type northern hardwoods (Table V) show small values of both r^2 and RMSE for height. This is a consequence of the relatively narrow range of average height within the sample population of 12 stands. The large sample size of the upland conifer species make these results significant at all levels of classification.

Table VI shows the net effect of the level of structural classification on the retrieval results for each biophysical parameter. The total number of stands decreases from 63 to 60 at finer levels of classification as some structural types (species) have very small sample populations (i.e., two white pine plantations). Results for such small populations have no statistical significance and are not reported. In general, the first two levels of structural classification, based upon growth form and growth form plus needle size, yield relatively poor rms errors for each variate. There is only marginal improvement between the two except for basal area where rms error improves from 11.3 m^2/ha to 6.5 m^2/ha when the excurrent trees are subclassified by needle-length. This is a consquence of two factors: 1) the short needle excurrent trees only constitute a small fraction of the sample population (i.e., 4 stands) but 2) the basal areas and height to diameter relationships of these lowland conifer species are very different from those of upland conifers.

Structural classification to the third level, that afforded by SIR-C/X-SAR, is found to yield significant improvement in the accuracy of the biophysical estimates. At this level of classification, the rms errors are found to be 2.4 m and 3.5 m^2/ha for height and basal area, respectively. The SAR-

TABLE V

Structure		Local Species Name	Biophysical Variate	Units	Equation	No. of Cases	r^2	RMSE
Group	Sub-Group							
A. Using SIR-C Data Only								
Decurrent	Large Branches	N. Hardwoods (Maple, Beech)	Height	m	$-1.476\sigma^{\circ}_{C,vv} - 0.712$	12	0.07	2.33
			Basal Area	m^2/ha	$0.912C_{\varsigma} + 34.009$	12	0.49	3.97
			Trunk Biomass	kg/m^2	$0.039\hat{h}\hat{b}_a - 3.343$	12	0.61	1.76
			Crown Biomass	kg/m^2	$0.229C_{\varsigma} + 3.767$	12	0.57	0.85
			Total Biomass	kg/m^2	$\hat{B}_c + \hat{B}_t$	12	0.64	2.38
Decurrent	Small Branches	Aspens	Height	m	$11.488(\sigma^{\circ}_{C,hh} - \sigma^{\circ}_{C,hv}) - 51.227$	5	0.94	0.89
			Basal Area	m^2/ha	$0.828C_{\varsigma} + 19.386$	5	0.79	2.99
			Trunk Biomass	kg/m^2	$0.028\hat{h}\hat{b}_a - 0.189$	5	0.95	0.64
			Crown Biomass	kg/m^2	$0.036C_{\varsigma} + 0.758$	5	0.99	0.25
			Total Biomass	kg/m^2	$\hat{B}_c + \hat{B}_t$	5	0.96	0.62
Excurrent	Small Branches, Small Needles	Lowland Conifers	Height	m	$1.162(\sigma^{\circ}_{L,vv} - \sigma^{\circ}_{C,hv}) + 12.012$	4	0.95	4.21
			Basal Area	m^2/ha	$-14.519(\sigma^{\circ}_{L,vv} - \sigma^{\circ}_{L,hv}) + 136.826$	4	0.63	0.62
			Trunk Biomass	kg/m^2	$0.135(\hat{h}\hat{b}_a)^{0.7115} - 1.179$	4	0.96	0.61
			Crown Biomass	kg/m^2	$0.971\sigma^{\circ}_{L,hv} + 17.394$	4	0.99	0.07
			Total Biomass	kg/m^2	$\hat{B}_c + \hat{B}_t$	4	0.97	0.65
Excurrent	Small Branches, Medium Needles	Upland Conifer (Jack Pine)	Height (1)	m	$26.423 * 10^{-0.192\left(\sigma^{\circ}_{L,vv}/\sigma^{\circ}_{L,hv}\right)}$	20	0.78	1.47
			Basal Area	m^2/ha	$2{,}308.02 * 10^{\left(0.128\sigma^{\circ}_{L,hv}\right)} - 1.23$	20	0.88	2.21
			Trunk Biomass	kg/m^2	$0.03\hat{h}\hat{b}_a - 0.162$	20	0.87	0.87
			Crown Biomass	kg/m^2	$0.416\sigma^{\circ}_{C,vv} + 5.929$	20	0.56	0.34
			Total Biomass	kg/m^2	$\hat{B}_c + \hat{B}_t$	20	0.89	0.93
Excurrent	Large Branches, Long Needles	Upland Conifer (Red Pine)	Height	m	$4.669\sigma^{\circ}_{L,vv} + 71.53$	19	0.89	3.45
			Basal Area	m^2/ha	$6.975\sigma^{\circ}_{L,hv} + 132.076$	19	0.87	4.26
			Trunk Biomass	kg/m^2	$0.011(\hat{h}\hat{b}_a)^{1.098} - 0.353$	19	0.96	0.98
			Crown Biomass	kg/m^2	$0.376(\sigma^{\circ}_{L,hv} - \sigma^{\circ}_{C,hh}) + 3.747$	19	0.88	0.32
			Total Biomass	kg/m^2	$\hat{B}_c + \hat{B}_t$	19	0.95	1.22
B. Using SIR-C/X-SAR Data								
Decurrent	Large Branches	N. Hardwoods (Maple, Beech)	Height	m	$3.246 * 10^{-0.145\left(\sigma^{\circ}_{L,hv} - \sigma^{\circ}_{X,vv}\right)} + 0.905$	8	0.56	1.24
Excurrent	Small Branches, Long Needles	Upland Conifer (Jack Pine)	Crown Biomass (1)	kg/m^2	$0.036 * 10^{2.588\left(\sigma^{\circ}_{C,hv}/\sigma^{\circ}_{X,vv}\right)} - 0.127$	7	0.87	0.23
Excurrent	Large Branches, Long Needles	Upland Conifer (Red Pine)	Crown Biomass	kg/m^2	$0.430(\sigma^{\circ}_{L,hv} - \sigma^{\circ}_{X,vv}) + 2.977$	8	0.96	0.24

notes: (1) σ° is in linear units.

derived estimates $\hat{b}_a$ and $\hat{h}$ are plotted versus the biometrically sampled b_a and the mean of allometrically estimated h in Fig. 9. The error bars shown are those determined by the measured within-stand variance in σ°, basal area and diameter (height is calculated allometrically from measured stem diameters). Approximately 90% of the forest stands are found to have estimated $\hat{b}_a$ and $\hat{h}$ that are within the 95% confidence interval around b_a and $\bar{h}$.

TABLE VI

$y = a\hat{y} + b$ $\quad RMSE = \left(\Sigma(y-\hat{y})^2 / N\right)^{1/2}$

CLASS TYPES	STRUCTURAL CLASSIFICATION LEVEL: DECURRENT EXCURRENT	DECURRENT EXCURRENT SHORT NEEDLE LONG NEEDLE	DECURRENT SMALL BRANCH LARGE BRANCH EXCURRENT SHORT NEEDLE LONG NEEDLE SMALL BRANCH LARGE BRANCH
No. of Classes	2	3	5
No. of Cases	63	61	60
Height r^2	0.367	0.653	0.895
a	1.0	1.0	0.995
b	-0.002	-0.002	0.094
RMSE (m)	5.57	4.02	2.38
Basal Area r^2	0.411	0.799	0.941
a	1.0	1.0	1.0
b	- 0.001	0.001	-0.008
RMSE (m^2/ha)	11.30	6.48	3.53
Trunk Biomass r^2	0.601	0.637	0.964
a	1.003	1.0	1.001
b	-0.029	0.0	-0.012
RMSE (kg/m^2)	3.80	3.49	1.11
Crown Biomass r^2	0.475	0.518	0.964
a	1.0	1.0	1.001
b	0.0	0.001	-0.012
RMSE (kg/m^2)	0.94	0.91	0.47
Total Dry Biomass r^2	0.573	0.632	0.958
a	1.0	0.992	0.985
b	0.242	0.204	0.260
RMSE (kg/m^2)	4.67	4.11	1.40

The estimates of dry biomass for the trunk, crown and aboveground total have rms errors of 1.1, 0.5, and 1.4 kg/m^2, respectively. The distributions of these errors are shown in Fig. 9. The error bars assume 20% uncertainty in the allometric estimation of biomass. The errors are randomly distributed over the entire range of biomass (up to 25 kg/m^2), indicating that "saturation effects" are not inhibiting estimate accuracy.

Having established that the preceding methodology can yield accurate estimates of forest biophysical properties, the approach can be applied in the image domain to create thematic maps at regional scales. This is is illustrated using the SIR-C data from the region including the Raco Supersite (Figs. 10 and 11). The *a priori* classification given in Fig. 2 is used to specify retrieval algorithms and their coefficients at the pixel level for height and basal area (Fig. 10). Crown biomass is estimated in a similar fashion [Fig. 11(a)]. Ancillary information concerning taper factor and wood density are combined with $\hat{b}_a$ and $\hat{h}$ to estimate trunk biomass [Fig. 11(b)]. Total biomass [Fig. 11(c)] is the summation of crown and trunk fractions.

These thematic maps are useful for regional ecosystem mapping and process models as well as for local resource management. In the region of the Raco Plain, for example, budworms have seriously damaged many of the jack pine stands. The susceptibility of jack pines to infestation is known to be a function of the local distributions of height and basal area. Hence, thematic maps of these two variates can be used to generate susceptibility maps to guide forest management plans.

The biomass map alone can be used to provide an estimate of the aboveground carbon pool. In addition, there is an opportunity to improve estimates of carbon flux since maintenance respiration can be calculated on the basis of the distribution of the woody biomass. Woody biomass is given as $B_t + X_i B_c$ where X_i is the allometrically derived fraction of the crown comprised of woody stems for the ith class.

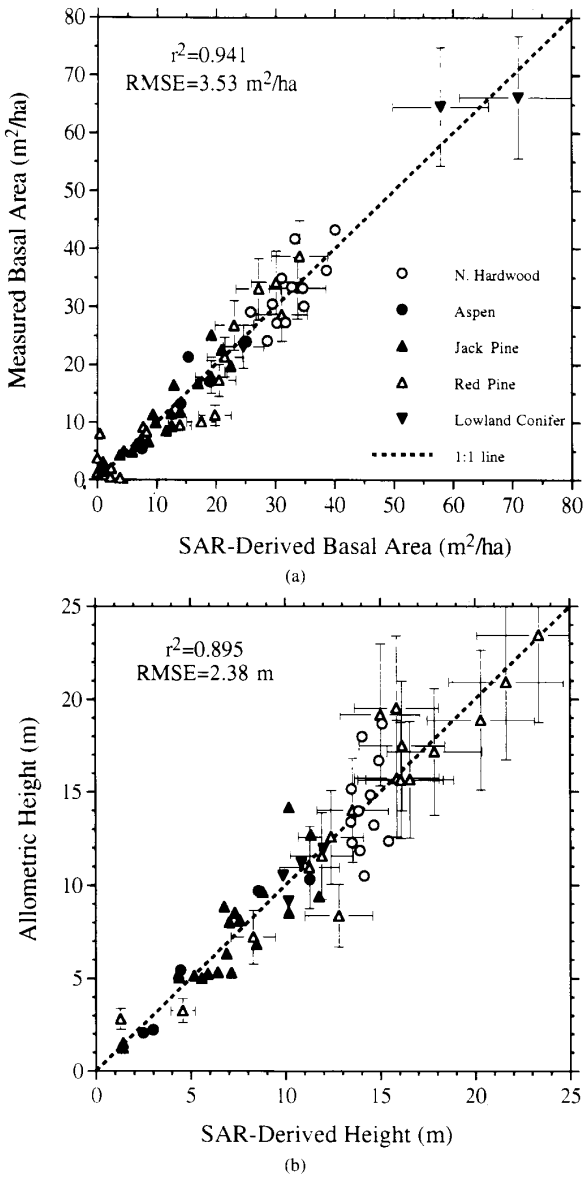

Fig. 8. Accuracy of SIR-C SAR-derived estimates of (a) basal area and (b) height.

C. Improvement Using SIR-C/X-SAR

Due to misalignment between the SIR-C and X-SAR antennas [see Fig. 4(c)], only a fraction of the forest test stands at the Raco Supersite were imaged by X-SAR (59% of the deciduous stands and 37% of the coniferous stands). Within this limited data set, the optimum functions and coefficients for the estimation (11)-(14) are recalculated using SIR-C and X-SAR data. For those cases where the inclusion of X-SAR leads to an increase in r^2, the equations are included as subsections in Tables III-V. In all cases, X-SAR is only selected when used in combination with longer wavelength and cross-polarized data (usually L-band). The addition of X-SAR ratios is found to significantly reduce rms errors in estimates of height for

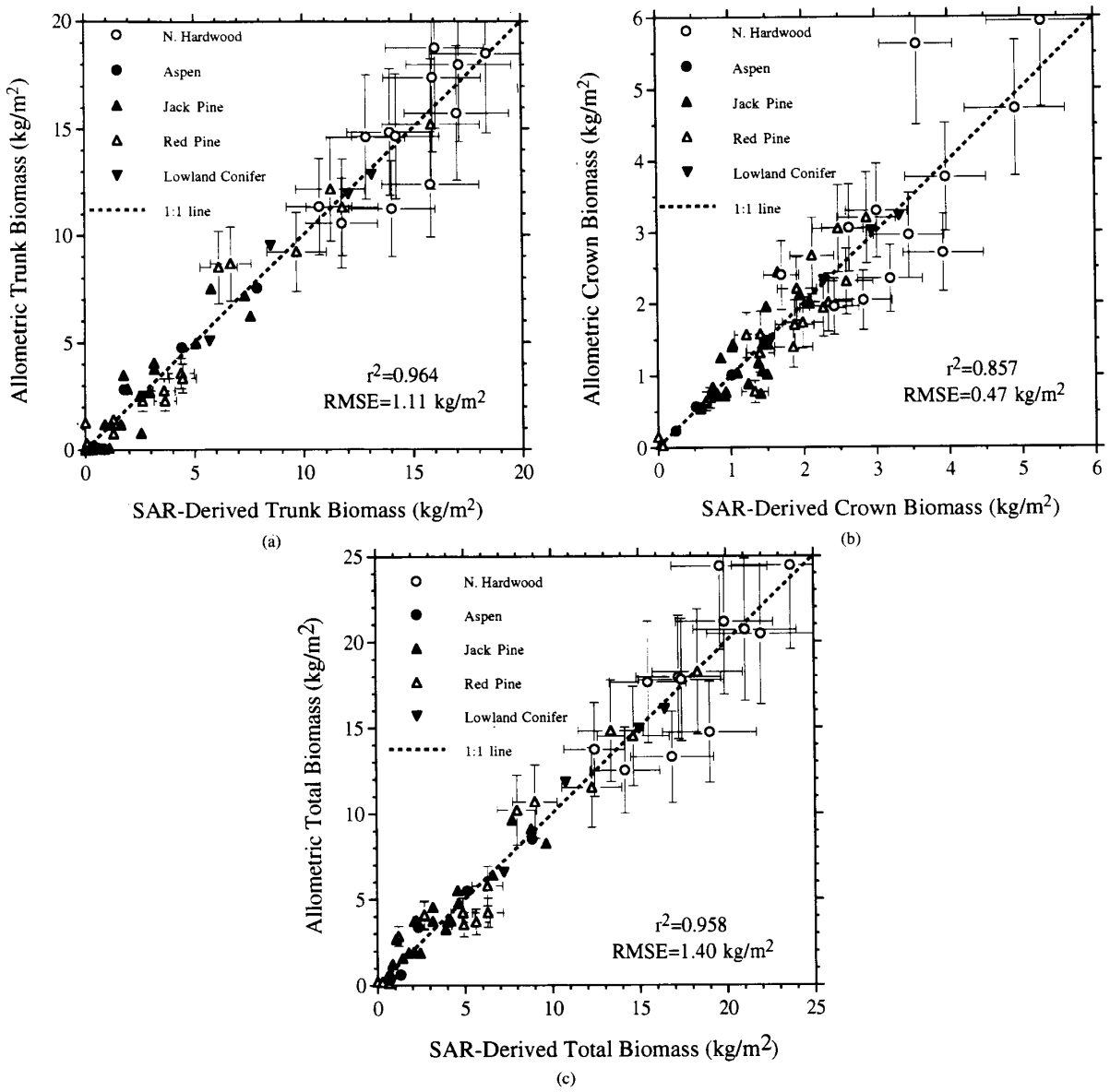

Fig. 9. Accuracy of SIR-C SAR-derived estimates of dry biomass: (a) trunk biomass, (b) crown biomass and (c) total biomass.

decurrent tree forms and also in estimates of crown biomass for excurrent tree forms.

However, the sample size is too small to evaluate the statistical significance of these results. This will have to be done using other X-SAR data takes from SRL-1 and SRL-2. The X-SAR data is not used to generate the results shown in Figs. 8–11.

V. Conclusion

In this study we have examined relatively simple approaches for retrieval of forest biophysical properties from orbital SAR data. In general, a power-law relationship is found to exist between σ° and dry biomass which saturates at biomass levels that scale with wavelength. The slope of this relationship and the saturation behavior are found to be controlled by forest structural attributes. As a result, simple direct retrieval of total dry biomass from σ° or multifrequency ratios is found to be ill-posed in our study area unless the effects of forest structure are taken into explicit account. A methodology for doing so is developed and tested using the SIR-C/X-SAR data obtained at the Raco Supersite during SRL-1 in April 1994.

This methodology uses a three-step process. First, a given terrain element is classified into a structural category on the basis of either 1) SAR-derived structural class (i.e., surface; short vegetation; tall vegetation subdivided by tree form, branch architecture and foliage characteristics) or 2) *a priori* classification by some other means. Secondly, polarimetric SAR data is used to empirically estimate primary structural

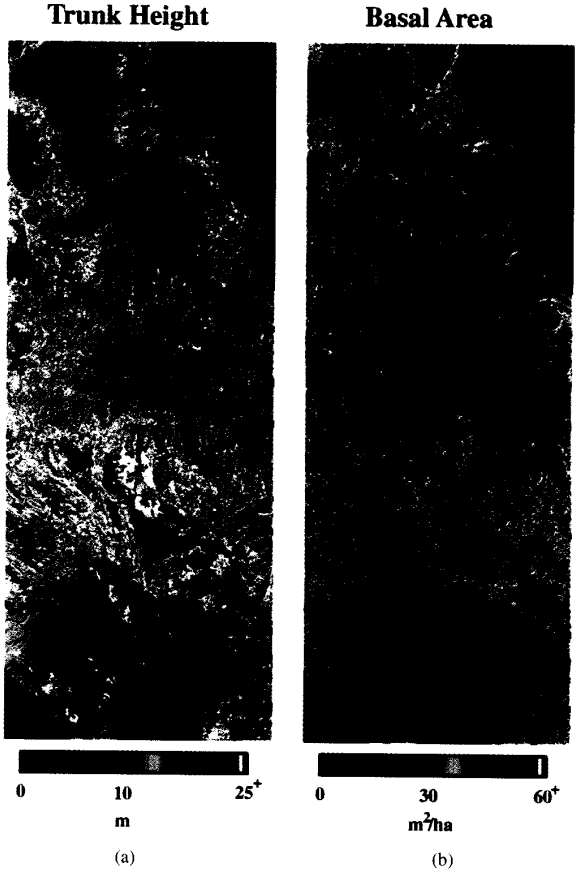

Fig. 10. Images of SIR-C SAR-derived (a) estimates of trunk height and (b) basal area in the Upper Peninsula of Michigan.

variates (basal area, height and crown biomass) of forested areas. The coefficients of the estimation algorithms are specific to each structural class. Lastly, trunk biomass is estimated from basal area and height using a simple biophysical model that requires commonly available information on trunk taper factor and the density of wood for each structural class. Net dry biomass is estimated as the sum of the trunk and crown biomass.

The methodology is tested using the SIR-C data alone and in combination with X-SAR data for three classification scenarios. In the first, only excurrent and decurrent tree forms are classified. In the second, the excurrent tree form is further subclassified on the basis of foliage structure (short versus long needles). The third scenario includes subclassification of both excurrent and decurrent tree forms on the basis of branch size (large and small). The accuracy of the retrieval process is found to be highly dependent upon the level of antecedent classification. For total dry biomass, the rms errors are found to be 4.7, 4.1, and 1.4 kg/m^2 for classifications levels 1 to 3, respectively when applied to the 60 or more test stands. These results are further improved by addition of X-SAR data, particularly the estimation of crown biomass. However, the statistical significance of this improvement cannot be fully evaluated due to a small sample size resulting from antenna misalignment. The testing population includes forest communities representative of both the boreal forest and the northern temperate forest. Total aboveground dry biomass ranges from 0 to 25 kg/m^2 for the sample population. In general, the SAR-derived estimate errors are on the order of those obtained by intensive biometric surveys of the test stand (a 10% area sample for trees greater than 5 m in height and a 3% area sample for trees less than 5 m in height).

The estimation equations make use of both the amplitude and relative phase information of SIR-C. In general, the shorter wavelengths (C- and X-band) alone or as ratios to L-band hv-polarized data yield the best estimation functions for crown biomass. Longer wavelength data, particularly L-band with hv-polarization, are best for estimation of trunk related properties (basal area and height) for excurrent tree forms. This is to be expected for tree types that produce strong bistatic returns from trunk and surface interaction. Although these decurrent tree species all have large and near-vertical trunks, higher frequency data at C-band is generally selected for estimation of trunk-layer attributes. This result indicates that the trunk-layer structural attributes are being inferred from crown-layer properties with which they are highly correlated. Relatively poor correlations between L-band backscatter and height indicates that the large branch elements in the crown are the dominant scatterers at this wavelength. This also explains the higher rms errors found for the decurrent tree forms relative to the excurrent forms.

The estimation functions are applied in the image domain to illustrate the landscape patterns of the derived properties over an ecophysiological gradient. The lateral and temporal extensibility of the specific estimation functions obtained in the study are limited by two sets of factors. First, there are sensor-related factors given by SAR calibration. In this study we have used the standard SIR-C/X-SAR single-look products with no additional post-processing calibration applied at the local scene level. Hence, any calibration errors inherent in this scene (or some other scene) will affect the equation coefficients. Secondly, there are several factors related to scene properties: 1) moisture or dielectric effects and 2) allometric relationships. The empirical approach used herein implicitly incorporates the dielectric properties of the vegetation and the underlying surface into the equation coefficients for each structural class. These are known to vary with time; and the extent to which these effect the equation coefficients is being evaluated using the remaining SIR-C/X-SAR images obtained in April and October 1994. During SRL-1 and 2 missions, the Raco Supersite experienced surface conditions including wet snow, dry snow, no snow, saturated soil to dry soil and vegetation conditions ranging from pre-emergence of deciduous shoots to senescence. These effects are the subject of continuing research and will be reported upon at a later date. In addition, lateral extensibility is affected by the regional nature of allometric relationships. Hence, locally derived allometric relatioships should be used where possible.

In spite of these caveats, this study shows that high accuracy retrievals of forest height, basal area, crown and trunk biomass are possible using SIR-C/X-SAR. While simple single frequency and polarization retrievals are limited by saturation effects, the multi-step approach used herein shows

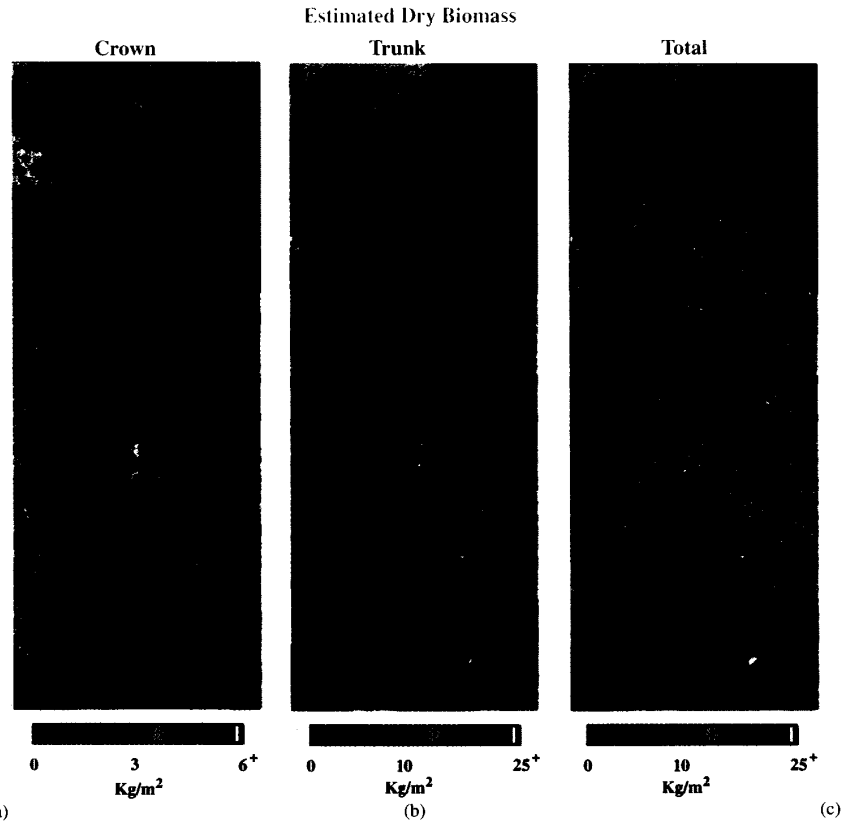

Fig. 11. Images of SIR-C SAR-derived estimates of dry biomass for (a) crown-layer, (b) trunk-layer and (c) total biomass.

retrievals are accurate up to at least 25 kg/m^2 for the forest communities studied. The challenge now lies in extending the approach regionally outside of the area of development and in applying the SAR-derived information to ecological and resource management problems.

ACKNOWLEDGMENT

The comments of the reviewers are also gratefully acknowledged.

REFERENCES

[1] P. J. Seller, Ed., *ISLSCP Workshop Report: Remote Sensing of the Land Surface for Studies of Global Change*, International Satellite Land Surface Climatology Project Workshop, Columbia, MD, June 23–26, 1992, NASA Goddard Space Flight Center, Greenbelt, MD, May 1993.

[2] R. E. Hunt, Jr., "Relationship between woody biomass and PAR conversion efficiency for estimating new primary production from NDVI," *Int. J. Remote Sensing*, vol. 15, no. 8, pp. 1725–1730, 1994.

[3] J. A. Richards, G. Sun, and D. S. Simonett, "L-band radar backscatter modeling of forest stands," *IEEE Trans. Geosci. Remote Sensing*, vol. GRS–25, pp. 487–498, 1987.

[4] S. L. Durden, J. J. van Zyl, and H. A. Zebker, "Modeling and observation of the radar polarization signature of forested areas," *IEEE Trans. Geosci. Remote Sensing*, vol. 27, pp. 290–301, 1989.

[5] F. T. Ulaby, K. Sarabandi, K. McDonald, M. Whitt, and M. C. Dobson, "Michigan microwave canopy scattering model," *Int. J. Remote Sensing*, vol. 11, no. 7, pp. 1223–1253, 1990.

[6] K. C. McDonald, M. C. Dobson, and F. T. Ulaby, "Using MIMICS to model L-band multiangle and multitemporal backscatter for a walnut orchard," *IEEE Trans. Geosci. Remote Sensing*, vol. 28, pp. 477–491, July 1990.

[7] ——, "Modeling multifrequency diurnal backscatter from a walnut orchard," *IEEE Trans. Geosci. Remote Sensing*, vol. 29, pp. 852–863, Nov. 1991.

[8] M. C. Dobson, L. E. Pierce, K. Sarabandi, F. T. Ulaby, and T. Sharik, "Preliminary analysis of ERS-1 SAR for forest ecosystem studies," *IEEE Trans. Geosci. Remote Sensing*, vol. 30, pp. 203–211, Mar. 1992.

[9] M. C. Dobson, F. T. Ulaby, and L. E. Pierce, "Land-cover classification and estimation of terrain attributes using synthetic aperture radar," *Remote Sensing Environ.*, vol. 51, no. 1, pp. 199–214, 1995.

[10] Y. Wang, F. W. Davis, and J. M. Melack, "Simulated and observed backscatter at P-, L-, and C-bands from ponderosa pine stands," *IEEE Trans. Geosci. Remote Sensing*, vol. 31, pp. 871–879, July 1993.

[11] A. Beaudoin, T. LeToan, S. Goze, E. Nezry, A. Lopes *et al.*, "Retrieval of forest biomass from SAR data," *Int. J. Remote Sensing*, vol. 15, no. 14, pp. 2777–2796, 1994.

[12] C. C. Hsu, H. C. Han, R. T. Shin, J. A. Kong, A. Beaudoin, and T. LeToan, "Radiative transfer theory for polarimetric remote sensing of pine forest at P-band," *Int. J. Remote Sensing*, vol. 15, no. 14, pp. 2943–2954, 1994.

[13] R. H. Lang, N. S. Chauhan, J. K. Ranson, and O. Kilic, "Modeling P-band SAR returns from a red pine stand," *Remote Sensing Environ.*, vol. 47, no. 2, pp. 132–141, 1994.

[14] S. H. Yueh, J. A. Kong, J. K. Jao, R. T. Shin, and T. LeToan, "Branching model for vegetation," *IEEE Trans. Geosci. Remote Sensing*, vol. 30, pp. 390–402, Mar. 1992.

[15] F. T. Ulaby, F. Kouyate, B. Brisco, and T. H. L. Williams, "Textural information in SAR images," *IEEE Trans. Geosci. Remote Sensing*, vol. GRS–24, pp. 235, Mar. 1986.

[16] G. Sun, D. S. Simonett, and A. H. Strahler, "A radar backscatter model for discontinuous coniferous forest canopies," *IEEE Trans. Geosci. Remote Sensing*, vol. 29, pp. 639–650, 1991.

[17] K. C. McDonald and F. T. Ulaby, "Radiative transfer modeling of discontinuous tree canopies at microwave frequencies," *Int. J. Remote Sensing*, vol. 14, no. 11, pp. 2097–2128, 1993.

[18] J. F. Weishampel, G. Sun, J. K. Ranson, D. LeJune, and H. H. Shugart, "Forest textural properties from simulated microwave backscatter: The

influence of spatial resolution," *Remote Sensing Environ.*, vol. 47, no. 2, pp. 120–131, 1994.
[19] G. Sun and K. J. Ranson, "A three-dimensional radar backscatter model of forest canopies," *IEEE Trans. Geosci. Remote Sensing*, vol. 33, pp. 372–382, Mar. 1995.
[20] E. Rignot and R. Chellappa, "Segmentation of polarimetric synthetic aperture radar data," *IEEE Trans. Image Proc.*, vol. 1, no. 3, p. 281, 1992.
[21] J. J. van Zyl and C. F. Burnette, "Baysian classification of polarimetric SAR images using adaptive a priori probabilities," *Int. J. Remote Sensing*, vol. 13, pp. 835–840, 1992.
[22] J. K. Ranson and G. Sun, "Northern forest classification using temporal multifrequency and multipolarimetric SAR images," *Remote Sensing Environ.*, vol. 47, no. 2, pp. 142–153, 1994.
[23] G. F. de Grandi, G. C. Lemoine, H. de Groof, C. Lavalle, and A. J. Sieber, "Fully polarimetric classification of the Black Forest MAESTRO 1 AIRSAR data," *Int. J. Remote Sensing*, vol. 15, no. 14, pp. 2755–2776, 1994.
[24] A. Lopes, E. Nezry, R. Touzi, and H. Laur, "Structure detection and statistical adaptive filtering in SAR images," *Int. J. Remote Sensing*, vol. 14, pp. 1735–1758, 1993.
[25] D. F. Lozano-Garcia and R. M. Hoffer, "Synergistic effects of combined Landsat-TM and SIR-B data for forest resources assessment," *Int. J. Remote Sensing*, vol. 14, no. 14, pp. 2677, 1993.
[26] E. J. M. Rignot, C. L. Williams, J. B. Way, and L. A. Viereck, "Mapping of forest types in Alaskan boreal forests using SAR imagery," *IEEE Trans. Geosci. Remote Sensing*, vol. 32, pp. 1051–1059, Sept. 1994.
[27] J. A. Drieman, "Forest cover typing and clearcut mapping in Newfoundland with C-band SAR," *Can. J. Remote Sensing*, vol. 20, pp. 11–16, 1994.
[28] G. M. Foody, M. B. McCulloch, and W. B. Yates, "Crop classification from C-band polarimetric radar data," *Int. J. Remote Sensing*, vol. 15, no. 14, pp. 2871–2886, 1994.
[29] J. J. van Zyl, "Unsupervised classification of scattering behavior using radar polarimetry data," *IEEE Geosci. Remote Sensing*, vol. 27, pp. 36–45, Jan. 1989.
[30] L. E. Pierce, F. T. Ulaby, K. Sarabandi, and M. C. Dobson, "Knowledge-based classification of polarimetric SAR images," *IEEE Trans. Geosci. Remote Sensing*, vol. 32, pp. 1081–1086, Sept. 1994.
[31] M. C. Dobson, L. E. Pierce, and F. T. Ulaby, "Knowledge-based land-cover classification using ERS-1/JERS-1 SAR composites," *IEEE Trans. Geosci. Remote Sensing*, submitted.
[32] F. T. Ulaby, L. Pierce, C. Dobson, S. Chacon and K. Sarabandi, "Land-cover classification by SAR," *Proc. IGARSS '94*, California Inst. Tech., Pasadena, Aug. 8–12, 1994.
[33] S. T. Wu, "Potential application of multipolarization SAR for pine-plantation biomass estimation," *IEEE Trans. Geosci. Remote Sensing*, vol. GRS-25, pp. 403–409, May 1987.
[34] S. A. Sader, "Forest biomass, canopy structure, and species composition relationships with multipolarization L-band synthetic aperture radar data," *Photogramm. Eng. Remote Sensing*, vol. 53, no. 2, pp. 193–202, 1987.
[35] G. Sun and D. S. Simonett, "Simulation of L-band HH microwave backscatter from coniferous forest stands: A comparison with SIR-B data," *Int. J. Remote Sensing*, vol. 9, pp. 907–925, 1988.
[36] M. C. Dobson, F. T. Ulaby, T. LeToan, A. Beaudoin, E. S. Kasischke, and N. Christensen, "Dependence of radar backscatter on coniferous forest biomass," *IEEE Trans. Geosci. Remote Sensing*, vol. 30, pp. 412–415, Mar. 1992.
[37] T. LeToan, A. Beaudoin, J. Riom, and D. Guyon, "Relating forest biomass to SAR data," *IEEE Trans. Geosci. Remote Sensing*, vol. 30, pp. 403–411, Mar. 1992.
[38] Y. Wang, F. W. Davis, and J. M. Melack, "Simulated and observed radar backscatter at P-, L- and C-bands from ponderosa pine stands," *IEEE Trans. Geosci. Remote Sensing*, vol. 31, pp. 871–879, 1993.
[39] Y. Wang, J. L. Day, F. W. Davis, and J. M. Melack, "Modeling L-band radar backscatter from Alaskan boreal forest," *IEEE Trans. Geosci. Remote Sensing*, vol. 31, pp. 1146–1154, 1993.
[40] M. Moghaddan, S. Durden, and H. Zebker, "Radar measurements of forested areas during OTTER," *Remote Sensing Environ.*, vol. 47, pp. 154–166, 1994.
[41] J. B. Way, E. J. M. Rignot, K. C. McDonald, R. Oren, R. Kwok *et al.*, "Evaluating the type and state of Alaska taiga forests with imaging radar for use in ecosystem models," *IEEE Trans. Geosci. Remote Sensing*, vol. 32, pp. 353–370, Mar. 1994.
[42] K. J. Ranson and G. Sun, "Mapping biomass of a northern forest using multifrequency SAR data," *IEEE Trans. Geosci. Remote Sensing*, vol. 32, pp. 388–396, May 1994.
[43] M. L. Imhoff, "A theoretical analysis of the effect of forest structure on synthetic aperture radar backscatter and the remote sensing of biomass," *IEEE Trans. Geosci. Remote Sensing*, vol. 33, pp. 341–352, Mar. 1995.
[44] ——, "Radar backscatter and biomass saturation: Ramifications for global biomass inventory," *IEEE Trans. Geosci. Remote Sensing*, vol. 33, pp. 511–518, Mar. 1995.
[45] E. Rignot, J. B. Way, C. Williams, and L. Viereck, "Radar estimates of aboveground biomass in boreal forests of interior Alaska," *IEEE Trans. Geosci. Remote Sensing*, vol. 32, pp. 1117–1124, Sept. 1994.
[46] R. H. Waring, J. B. Way, R. Hunt Jr., L. Morrisey, J. K. Ranson, "Remote sensing with synthetic aperture radar in ecosystem studies," *Bioscience*, to appear.
[47] L. E. Pierce, M. C. Dobson, E. Wilcox, and F. T. Ulaby, "Artifical neural network inversion of tree canopy parameters in the presence of diversity," *IGARSS*, Aug. 18–21, 1993, Kogakuin Univ., Kyoto, Japan.
[48] M. H. Zimmerman and C. L. Brown, *Trees Structure and Function*. New York: Springer-Verlag, 1971.
[49] T. L. Sharik and I. D. Brodie, "Structure, composition and above-ground biomass of SIR-C/ERS-1 sample stands at Pellston and Raco, Michigan, USA, 1990–91," School of Forestry and Wood Products, Michigan Tech. Univ., Houghton, Contract Tech. Rep. 01, Nov. 1992.
[50] ——, "Structure, composition and above-ground biomass of SIR-C/ERS-1 sample stands at Raco, Michigan, USA, 1992," School of Forestry and Wood Products, Michigan Tech. Univ., Houghton, Contract Tech Rep. 02, July 1993.
[51] D. H. Alban and P. R. Laidly, "Generalized biomass equations for Jack Pine and Red Pine in the Lake States," *Can. J. For. Res.*, 12:913–921, 1982.
[52] I. S. Alemdag, "Aboveground dry matter of Jack Pine, Black Spruce, White Spruce and Balsam fir trees at two localities in Ontario," *For. Chron.*, vol. 58, pp. 26–30, 1982.
[53] T. R. Crow and G. G. Erdmann, "Weight and volume equations and tables for Red Maple in the Lake States," *USDA For. Serv. Res. Paper*, NC–242, 1978.
[54] D. F. Grigal and L. K. Kernik, "Generality of Black Spruce biomass equations," *Can. J. For. Res.*, vol. 14, pp. 68–470, 1984.
[55] M. F. Ker, "Tree biomass equations for seven species in Southwestern New Brunswick," Can. For. Serv. Marit. For. Res. Center Inf., Rep., M-X-114, 1980.
[56] G. J. Koerper and C. J. Richardson, "Biomass and net annual primary production regressions for *Populus grandidentata* for three sites in Northern Lower Michigan," *Can. J. For. Res.*, vol. 10, pp. 92–101, 1980.
[57] M. D. C. Schmitt and D. F. Grigal, "Generalized biomass estimation equations for Betula Papyrifera Marsh," *Can. J. For. Res.*, vol. 11, pp. 837–840, 1981.
[58] J. V. Wiant, Jr., F. Castaneda, C. E. Sheetz, A. Colaninno, and J. C. DeMoss, "Equations for predicting weights of some Appalachian hardwoods," *West Viginia. Univ. Agricult. For. Exp. Sta. Bulletin*, 659–T, pp. 1–36, 1979.
[59] D. C. Grenen and D. F. Grigal, "Generalized biomass equations for Jack Pine (*Pinus banksiana Lamb.*)," *Minnesota For. Res. Notes*, no. 268, p. 4, 1978.
[60] D. A. Perala and D. H. Alban, "Allometric biomass estimations for aspen-dominated ecosystems in the Upper Great Lakes," *USDA Forest Service Res. Paper*, North Central Experiment Station, 1993.
[61] K. Sarabandi, L. Pierce, M. C. Dobson, F. T. Ulaby, J. Stiles *et al.*, "Polarimetric calibration of SIR-C using point and distributed targets," *IEEE Trans. Geosci. Remote Sensing*, pp. 858–866, this issue.
[62] K. Sarabandi, "Derivation of phase statistics of distributed targets from the Mueller matrix," *Radio Sci.*, vol. 27, pp. 1349–1377, 1991.
[63] K. M. Bergen, M. C. Dobson, L. E. Pierce, J. L. Kendra, J. Kellndorfer, and P. Siqueira, "Apr. 1994 SIR-C/X-SAR mission: Ancillary data report Raco, Michigan site," *Radiation Lab Tech. Rep., 036511-5-T*, Radiation Lab, EECS Dept., The University of Michigan, Ann Arbor, MI, Dec. 1994.
[64] G. T. Ruck, D. E. Barrick, W. D. Stuart, and C. K. Krichbaum, *Radar Cross Section Handbook*. New York: Plenum Press, 1970.

M. Craig Dobson, for photograph and biography, please see p. 866 of this issue.

Fawwaz T. Ulaby (M'68–SM'74–F'80), for a photograph and biography, see p. 866 of this issue.

Leland E. Pierce (S'85–M'85), for a photograph and biography, see p. 866 of this issue.

T. L. Sharik, photograph and biography not available at the time of publication.

K. M. Bergen, photograph and biography not available at the time of publication.

J. Kellndorfer, photograph and biography not available at the time of publication.

J. R. Kendra, photograph and biography not available at the time of publication.

E. Li, photograph and biography not available at the time of publication.

Y. C. Lin, photograph and biography not available at the time of publication.

A. Nashashibi, photograph and biography not available at the time of publication.

Kamal Sarabandi (M'90–SM'92), for photograph and biography, please see p. 866 of this issue.

P. Siqueira, photograph and biography not available at the time of publication.